Hindawi
Geofluids
Volume 2019, Article ID 3041037, 16 pages
https://doi.org/10.1155/2019/3041037

Research Article

Degassing at the Volcanic/Geothermal System of Kos (Greece): Geochemical Characterization of the Released Gases and CO_2 Output Estimation

Kyriaki Daskalopoulou,[1,2] **Antonina Lisa Gagliano**,[3] **Sergio Calabrese**,[1,3] **Lorenza Li Vigni**,[3] **Manfredi Longo**,[3] **Konstantinos Kyriakopoulos**,[2] **Giovannella Pecoraino**,[3] **and Walter D'Alessandro**[3]

[1]*Università degli Studi di Palermo, Dipartimento di Scienze della Terra e del Mare, via Archirafi, 36, 90123 Palermo, Italy*
[2]*National and Kapodistrian University of Athens, Department of Geology and Geoenvironment, Panepistimioupolis, Ano Ilisia, 15784 Athens, Greece*
[3]*Istituto Nazionale di Geofisica e Vulcanologia, Sezione di Palermo, via Ugo la Malfa 153, 90146 Palermo, Italy*

Correspondence should be addressed to Walter D'Alessandro; walter.dalessandro@ingv.it

Received 10 December 2018; Accepted 2 April 2019; Published 26 June 2019

Guest Editor: Andrzej Solecki

Forty-five gas samples have been collected from natural gas manifestations at the island of Kos—the majority of which are found underwater along the southern coast of the island. On land, two anomalous degassing areas have been recognized. These areas are mainly characterized by the lack of vegetation and after long dry periods by the presence of sulfate salt efflorescence. Carbon dioxide is the prevailing gas species (ranging from 88 to 99%), while minor amounts of N_2 (up to 7.5%) and CH_4 (up to 2.1%) are also present. Significant contents of H_2 (up to 0.2%) and H_2S (up to 0.3%) are found in the on-land manifestations. Only one of the underwater manifestations is generally rich in N_2 (up to 98.9%) with CH_4 concentrations of up to 11.7% and occasionally extremely low CO_2 amounts (down to 0.09%). Isotope composition of He ranges from 0.85 to 6.71 R/R_A, indicating a sometimes-strong mantle contribution; the highest values measured are found in the two highly degassing areas of Paradise beach and Volcania. C-isotope composition of CO_2 ranges from -20.1 to 0.64‰ vs. V-PDB, with the majority of the values being concentrated at around -1‰ and therefore proposing a mixed mantle—limestone origin. Isotope composition of CH_4 ranges from -21.5 to +2.8‰ vs. V-PDB for C and from -143 to +36‰ vs. V-SMOW for H, pointing to a geothermal origin with sometimes-evident secondary oxidation processes. The dataset presented in this work consists of sites that were repeatedly sampled in the last few years, with some of which being also sampled just before and immediately after the magnitude 6.6 earthquake that occurred on the 20th of July 2017 about 15 km ENE of the island of Kos. Changes in the degassing areas along with significant variations in the geochemical parameters of the released gases were observed both before and after the seismic event; however, no coherent model explaining those changes was obtained. CO_2 flux measurements showed values of up to about 10_4 g × m^{-2} × d^{-1} in both the areas of Volcania and Kokkino Nero, 5×10^4 g × m^{-2} × d^{-1} at Paradise beach, and 8×10^5 g × m^{-2} × d^{-1} at Therma spring. CO_2 output estimations gave values of 24.6, 16.8, 12.7, and 20.6 t × d^{-1}, respectively, for the above four areas. The total output of the island is 74.7 t × d^{-1} and is comparable to those of the other active volcanic/geothermal systems of Greece (Nisyros, Nea Kameni, Milos, Methana, and Sousaki).

1. Introduction

The southern Aegean Sea is one of the most tectonically active regions of western Eurasia, where fast convergence of the Aegean microplate and the Eastern Mediterranean lithosphere (the front part of the African plate) occurs. The African plate subducts underneath the Aegean-Anatolian microplate at a rate of about 1 cm/a [1, 2], and the microplate

overrides the Eastern Mediterranean [3], resulting also in the generation of a volcanic arc [4]. The South Active Aegean Volcanic Arc (SAAVA) was built on Paleozoic-Mesozoic basement rocks (Alpine basement) that were deformed during the Tertiary by the Hellenide orogeny [5]. During the Lower Pliocene, the rate of convergence between the two continental margins increased and initiated the volcanism and the development of several hydrothermal systems at the SAAVA (e.g., [4, 6–10]).

Kos island is part of the Kos-Nisyros-Gyali volcanic system of the SAAVA, located at the SE edge of the Aegean Sea and formed at around 5 Ma, at the beginning of the Pliocene [1, 3, 11–13]. The geologic units of Kos consist of alluvial deposits with greenschists and flysch in the northern part of the island, lacustrine and terrestrial deposits of the Pliocene age in the central part with tuffs, and ignimbrites of the Quaternary age that cover the southern part of the island [14]. The most prominent volcanic formation on the island is the Kos Plateau Tuff (KPT). It is related to a caldera formed by an explosive eruption that occurred 161 ka ago, which is considered to be the largest explosive Quaternary eruption in the Eastern Mediterranean [15]. The tectonic evolution of the island is controlled by the dominant WNW-ESE and NE-SW faults, which are related to extensional processes and volcanic activity that took place during the Pleistocene and Pliocene [16, 17]. The volcanic island of Kos has been active for at least 3 million years [18] and continued to be active until recent times (e.g., [4, 6–10]). Some geothermal areas of particular interest have been identified in the island. The Volcania area is located 1 km northeast from the rim of Kefalos caldera [19]. It consists of a 1 km diameter basin with 14 small circular areas with evident signs of present and/or past hydrothermal alteration mainly arranged along two intersecting lineaments. These areas (5-20 m across) are devoid of vegetation and are usually covered by whitish altered deposits that contain sulfates and occasionally native sulfur [19]. Furthermore, hydrothermal activity is noticeable along the island with the most important sites being (i) the thermal spring of Therma, which is emerging on the beach close to Cape Fokas [20], (ii) the ferruginous spring of Kokkino Nero rich in CO_2 [21], and (iii) the intensively degassing area of Paradise beach at Kefalos Bay.

Geogenic carbon emissions have a critical impact on the carbon cycle [22, 23] and are regarded as one of the reasons of global climate changes on long time scales. Gas emissions from such sources strongly contribute to the increasing concentrations of greenhouse gases in the atmosphere, with methane and carbon dioxide playing a fundamental role [24, 25]. Moreover, earth degassing defines relations among flux, tectonic structures [26, 27], and volcanic activity [28, 29]. The aim of this study is to estimate the total CO_2 output of Kos island and to investigate the possible relation of these manifestations and anomalous areas with the geodynamically active area of Greece. This work presents new chemical and isotope data about the main gas manifestations of the island both on land and underwater. The collected data are interpreted together with literature data in order to determine the origin of the gases and the postgenetic processes that affect them. Finally, some considerations about possible variations on gas geochemistry induced by the earthquake ($M_w = 6.6$) on the 20th of July 2017 with an epicenter close to the island are made.

2. Methods

Bubbling gases of Kos island were sampled using an inverted funnel positioned above the emission point of the highest flux, whereas soil gases were collected by inserting a pipe in the soil at >50 cm in depth and driving the gas by a syringe and a 3-way valve. Dry gases were collected in glass flasks equipped with two stopcocks.

In the laboratory, the concentrations of He, H_2, H_2S, O_2, N_2, CO_2, and CH_4 on the samples were analysed by an Agilent 7890B gas chromatograph combined with a Micro GC analyser by INFICON. A single amount of gas sample is simultaneously split into the loops of the two combined systems. Concentrations of CO_2 and H_2S have been determined by the Micro GC analyser with He as the carrier and equipped with a PoraPLOT U column and TCD detector while all the other gases had been determined by the GC system with Ar as the carrier and equipped with a 4 m Carbosieve S II column. A TCD detector was used to measure the concentrations of He, H_2, O_2, and N_2 and a FID detector for that of CH_4. The analytical errors were less than 10% for He and less than 5% for the remaining gases.

The $^{13}C/^{12}C$ ratios of CO_2 (expressed as δ^{13}C-CO_2‰ V-PDB) were measured with a Finnigan Delta S mass spectrometer after purification of the gas mixture by standard procedures using cryogenic traps (precision $\pm 1\sigma = 0.1$‰). Carbon and hydrogen isotopes of CH_4 were measured using a Thermo TRACE GC interfaced to a Delta Plus XP gas source mass spectrometer and equipped with a Thermo GC/C III (for carbon) and with GC/TC peripherals (for hydrogen). The $^{13}C/^{12}C$ ratios are reported as δ^{13}C-CH_4 values with respect to the V-PDB standard ($\pm 1\sigma = 0.2$‰) while the $^{2}H/^{1}H$ ratios are reported as δ^{2}H-CH_4 values with respect to the V-SMOW standard ($\pm 1\sigma = 2.0$‰).

The abundance and isotope composition of He, and the $^{4}He/^{20}Ne$ ratios, were determined by separately admitting He and Ne into a split flight tube mass spectrometer (Helix SFT). Helium isotope compositions are given as R/R_A, where R is the ($^{3}He/^{4}He$) ratio of the sample and R_A is the atmospheric ($^{3}He/^{4}He$) ratio ($R_A = 1.386 \times 10^{-6}$). The analytical errors were generally <1%. The $^{4}He/^{20}Ne$ ratio was used to correct the measured values for the atmospheric contamination, and the corrected values are indicated as R_C/R_A [30]. The analytical results of the collected samples as well as their coordinates are presented in Table 1.

Flux maps were drawn according to the dataset obtained from the three field campaigns that took place in the period from October 2015 to October 2017 (Table 2). Measurements were always made during dry and stable weather conditions. CO_2 flux was measured at Volcania, Kokkino Nero, Paradise beach, and Therma with the accumulation chamber method at more than 600 sites (>500 points per km^2) with portable soil fluxmeters (West Systems, Italy) based on the accumulation chamber method [31]. Flux values were determined at each site from the rate of CO_2 concentration increase in the

Table 1: Coordinates and analytical results of the collected gas samples.

No.	Sample	Sector	Coordinates E	Coordinates N	Date dd-mm-yy	He	H_2	O_2	N_2	CH_4	CO_2	H_2S	R/R_A	$^4He/^{20}Ne$	$\delta^{13}C\text{-}CO_2$	$\delta^{13}C\text{-}CH_4$	$\delta^2H\text{-}CH_4$
									μmol/mol						‰ vs. V-PDB		‰ vs. V-SMOW-
1	Therma	35S	528211	4077679	14-04-10	<3	<2	1700	13100	70	958000	n.d.	n.d.	n.d.	n.d.	n.d.	n.d.
2	Therma	35S	528211	4077679	05-09-10	27	<2	660	44700	290	930000	n.d.	n.d.	n.d.	-3.35	2.8	n.d.
3	Therma	35S	528211	4077679	19-03-14	2.43	<2	1100	8900	50	995000	<5	1.04	2.92	-3.11	n.d.	n.d.
4	Therma	35S	528211	4077679	29-09-16	2.5	<2	530	9300	64	989000	<5	1.44	40.6	-3.46	2.4	36
5	Therma	35S	528211	4077679	26-07-17	7	1.6	1800	19100	110	982000	<5	1.39	23.0	-1.12	n.d.	n.d.
6	Therma	35S	528211	4077679	14-10-17	16	<2	2000	33100	210	949000	<5	1.49	30.5	-3.28	n.d.	n.d.
7	Therma	35S	528211	4077679	27-08-18	9.2	<2	1300	23800	160	958000	n.d.	1.45	55.7	-2.50	n.d.	n.d.
8	Therma Sea	35S	528211	4077679	29-09-16	16	<2	2500	42400	280	955000	<5	1.55	44.1	-3.04	n.d.	n.d.
9	Paradise	35S	500794	4068393	07-09-09	17	<2	3200	10800	11300	953000	n.d.	6.60	25.6	-1.06	n.d.	n.d.
10	Paradise	35S	500794	4068393	03-09-10	12	<2	790	3600	9300	966000	n.d.	6.59	43.9	-0.60	-19.8	n.d.
11	Paradise	35S	500794	4068393	13-09-11	14	2	190	4100	9700	986000	n.d.	6.66	27.8	-0.98	n.d.	n.d.
12	Paradise	35S	500794	4068393	20-08-12	28	<2	14700	34400	20900	900000	n.d.	6.67	34.1	-0.33	n.d.	n.d.
13	Paradise	35S	500794	4068393	13-06-13	12	<2	<100	3400	10000	968000	n.d.	6.70	112	-0.94	n.d.	n.d.
14	Paradise	35S	500794	4068393	20-03-14	23	<2	8400	19600	19200	937000	<5	6.55	49.0	-0.76	-19.5	n.d.
15	Paradise	35S	500794	4068393	27-09-15	14	<2	3100	8600	12100	959000	<5	6.49	223	-0.11	-19.5	-136
16	Paradise	35S	500794	4068393	29-09-16	12	<2	1700	5800	10000	980000	<5	6.27	270	-0.92	-20.1	-122
17	Paradise	35S	500794	4068393	30-09-16	17	<2	1800	8800	12100	972000	<5	n.d.	n.d.	-1.06	-20.0	-126
18	Paradise	35S	500794	4068393	30-09-16	16	<2	2200	7300	11000	977000	<5	n.d.	n.d.	-0.87	-20.6	-133
19	Paradise	35S	500794	4068393	30-09-16	12	<2	800	4100	9700	987000	<5	n.d.	n.d.	-1.82	n.d.	n.d.
20	Paradise	35S	500794	4068393	26-07-17	14	9	13300	46900	10800	915000	<5	6.71	90.7	-1.04	n.d.	n.d.
21	Paradise	35S	500794	4068393	14-10-17	21	2.2	6700	23200	15700	931000	<5	6.53	269	-0.67	-20.1	-124
22	Kokkino Nero	35S	521902	4078954	05-09-10	<3	<2	50	12300	520	966000	n.d.	n.d.	n.d.	-3.13	-21.5	n.d.
23	Kokkino Nero	35S	521902	4078954	19-03-14	5	3.1	3200	13600	3000	978000	<5	2.39	12.78	-1.94	-18.3	n.d.
24	Kokkino Nero	35S	522116	4078886	19-03-14	4.3	30	2700	8300	3100	991000	<5	n.d.	n.d.	n.d.	n.d.	n.d.
25	Kokkino Nero	35S	522116	4078886	29-09-15	5	<2	120	7200	3200	974000	36	n.d.	n.d.	-1.46	-19.5	-143
26	Kokkino Nero	35S	522116	4078886	29-09-16	6	<2	150	10500	3600	994000	<5	n.d.	n.d.	-1.43	-20.0	-104
27	Kokkino Nero	35S	522116	4078886	26-07-17	7	<2	1200	22600	3600	969000	<5	n.d.	n.d.	-1.70	n.d.	n.d.
28	Kokkino Nero	35S	522116	4078886	15-10-17	5	<2	1500	14500	3000	967800	<5	2.48	3.99	-1.48	-21.1	-92
29	Kokkino Nero	35S	521911	4075842	19-03-14	3.3	295	3500	24400	2400	980000	673	n.d.	n.d.	-0.97	-18.2	n.d.
30	Kokkino Nero	35S	521911	4075842	29-09-15	4	2.3	530	4000	2700	972000	2700	n.d.	n.d.	-2.09	n.d.	n.d.
31	Kefalos	35S	497339	4065831	28-09-15	24	15	3700	33000	25700	906000	<5	5.60	92.9	-0.59	-9.9	-71
32	Kefalos	35S	497339	4065831	29-09-16	18	27	3294	25100	23900	946000	<5	6.21	92.8	0.64	-12.2	-54
33	Kefalos	35S	497339	4065831	14-10-17	18	95	5800	35300	24200	902000	<5	6.01	192	-0.68	-12.4	-66
34	Agia Irini	35S	520916	4075676	28-09-15	0.94	<2	2600	6600	40	970000	15	0.85	5.86	-2.52	n.d.	n.d.
35	Agia Irini	35S	520916	4075676	30-09-16	0.34	<2	6219	14600	42	968000	<5	2.19	1.35	-2.24	n.d.	n.d.

Table 1: Continued.

No.	Sample	Sector	Coordinates E	Coordinates N	Date dd-mm-yy	He	H_2	O_2	N_2	CH_4	CO_2	H_2S	R/R_A	$^4He/^{20}Ne$	$\delta^{13}C\text{-}CO_2$	$\delta^{13}C\text{-}CH_4$	$\delta^2H\text{-}CH_4$
						μmol/mol									‰ vs. V-PDB		‰ vs. V-SMOW-
36	Agia Irini	35S	520916	4075676	16-10-17	0.90	<2	9500	26800	97	956000	<5	1.57	0.61	-2.11	n.d.	n.d.
37	Agia Irini spring	35S	520916	4075676	16-10-17	<3	<2	8900	36000	330	947000	<5	n.d.	n.d.	-3.21	n.d.	n.d.
38	Agia Irini 2	35S	521910	4075843	28-09-15	412	<2	2000	613000	117000	256000	<5	3.67	81.5	-0.82	-16.1	-75
39	Agia Irini 2	35S	521910	4075843	30-09-16	446	<2	2200	989000	6200	900	<5	3.88	48.2	-20.1	-12.4	-14
40	Agia Irini 2	35S	521910	4075843	16-10-17	220	<2	2600	343000	82900	548000	<5	3.62	66.2	-1.52	n.d.	n.d.
41	Volcania	35S	499783	4068858	27-09-15	36	65	810	30500	20600	926000	62	n.d.	n.d.	-0.43	-14.0	-115
42	Volcania	35S	499783	4068858	27-09-15	44	49	340	12400	23500	943000	1200	n.d.	n.d.	-0.55	-19.0	-132
43	Volcania	35S	499783	4068858	27-09-15	44	2.9	310	4000	23100	947000	851	6.71	1066	-0.50	-18.0	-128
44	Volcania	35S	499783	4068858	20-03-14	34	1980	10100	75400	21000	877000	54	n.d.	n.d.	0.25	n.d.	n.d.
45	Volcania	35S	499783	4068858	16-10-17	19	26	13000	74800	14500	882000	<5	5.73	8.94	-0.51	-14.1	-110

n.d.: not determined.

Table 2: Statistics on the populations identified in the CO_2 flux dataset.

Site	Pop.	Count	Min	Max	Mean	St. dev.
			Log CO_2 ($g \times m^{-2} \times d^{-1}$)			
Volcania	A	19	-1.000	0.763	0.362	0.446
	B	405	0.778	3.332	2.147	0.641
	C	16	3.423	4.001	3.619	0.183
Kokkino Nero	A	22	-0.356	1.289	0.818	0.378
	B	95	1.378	3.464	2.572	0.594
	C	13	3.534	4.158	3.786	0.219
Therma	B	13	1.127	4.024	2.755	0.845
	C	17	4.042	5.953	4.793	0.603
Paradise	C	12	2.754	4.726	4.031	0.604

chamber and are expressed in grams per square meter per day ($g \times m^{-2} \times d^{-1}$) after conversion from volumetric to mass concentrations considering atmospheric pressure and temperature values. IR spectrometers with different measurement ranges (0 – 20 $mmol \times mol^{-1}$ for the Licor LI820 and double range of 0 – 10 $mmol \times mol^{-1}$ and 0 – 1000 $mmol \times mol^{-1}$, respectively, for the Dräger Polytron) were used. This resulted in a measuring range of 10 – 20000 $g \times m^{-2} \times d^{-1}$ for the Licor LI820 spectrometer with accumulation chamber A and a range of up to 900000 $g \times m^{-2} \times d^{-1}$ for the Dräger Polytron spectrometer with accumulation chamber B and high measuring range—the reproducibility being always better than 20%. Chamber A has an area of 0.031 m^2 and a volume of 0.0028 m^3, while chamber B has the same area and a volume of 0.0062 m^3. Particular care was taken to follow the recommendations for flux measurements in volcanic/-geothermal environments made by Lewicki et al. [32].

The soil temperature was measured only at few places and only in the last campaign by means of a digital thermocouple (error ± 0.3°C in the range from -100 to 200°C).

The CO_2 datasets acquired from Volcania, Kokkino Nero, and Therma were used to estimate the total CO_2 flux from these areas.

To define the CO_2 threshold value, CO_2 flux data were processed following the Sinclair's portioning method extracting the main populations (Table 2; [33]). This method consists in the definition of single populations through the inflection points (main populations) or changes in direction (secondary populations) of the curvature on the probability plot by visual analysis.

Following the stochastic simulation approach, CO_2 flux maps were drawn. The data were converted by normal score transformation to follow a Gaussian distribution. The normal score transformed data was used to compute omnidirectional variograms and interpolated with the sequential Gaussian simulation (sGs) method by using the executable "sgsim" of GSLIB [34] and performing 100 equiprobable realizations for each area. The grid resolution was 5 × 5 m. The final maps were produced averaging the results of the 100 realizations, using the E-type postprocessing method.

Zonal Statistics on the three CO_2 flux maps, performed by using the ArcMap 10.3 (ESRI) Spatial Analyst tool, was used to estimate the total CO_2 output considering only flux values above the background threshold value for each area.

3. Results

In the period from 2009 to 2017, 10 sampling campaigns took place in the island of Kos and 45 gas samples were collected. Twenty-three of them were collected underwater at various depths (<10 m; Figure 1); five are soil gases whereas the remaining ones are gases bubbling in thermal waters. Literature data were also taken into consideration for comparison [14, 35, 36]. Names, sampling date, coordinates, chemical concentrations, and isotope values are presented on Table 1. Additionally, during the last three campaigns, more than 600 CO_2 flux measurements were performed covering part of the island (both on land and on the sea surface) including 4 intensively degassing areas: 135000 m^2 in Volcania (445 points), 250000 m^2 in Kokkino Nero (133 points), 1100 m^2 in Therma (29 points), and 600 m^2 in Paradise beach (12 points). Results of the flux measurements are presented in Table S1.

3.1. Gas Geochemistry. Gases collected from Kos island show that CO_2 is the prevailing gas species (generally more than 800000 $\mu mol \times mol^{-1}$ and up to 995000 $\mu mol \times mol^{-1}$; Figure 2). The majority of these samples display N_2/O_2 ratios higher than those of air and/or air-saturated water (ASW), indicating that the atmospheric component of meteoric water has been modified by redox reactions that took place either in the subsoil or in the aquifers. However, few samples present high concentrations of atmospheric gases (O_2 up to 99000 $\mu mol \times mol^{-1}$ and N_2 up to 989000 $\mu mol \times mol^{-1}$), pointing to a strong contamination by an atmospheric component (Figure 2(b)). Helium ranges from 0.34 to 511 $\mu mol \times mol^{-1}$, while CH_4 ranges from 40 to 118000 $\mu mol \times mo l^{-1}$. Hydrogen and H_2S, typical hydrothermal gases, present significant concentrations (up to 1900 and 2700 $\mu mol \times mo l^{-1}$, respectively) in the soil gases, whereas in the underwater emissions, they are mostly below detection limits.

The isotope composition of He shows values from 0.85 to 6.71 R/R_A with the highest values being found in the Paradise beach samples. Regarding the $^4He/^{20}Ne$ ratio, values of up to 1066 are observed. Carbon isotope composition of CO_2 in the island is in the range of -20.07 to +0.64‰ vs. V-PDB, although almost all samples fall within a narrower range (-3.5 and 0‰). The isotope composition of CH_4 varies from -21.5 to -2.8‰ vs. V-PDB for C and from -143 to +36‰ vs. V-SMOW for H.

3.2. CO_2 Fluxes and Soil Temperatures. CO_2 flux measurements for the areas under investigation gave values that range from <0.1 to 898000 $g \times m^{-2} \times d^{-1}$. The highest values were measured in Paradise beach and Therma spring (median 9540 and 15100; maximum 23100 and 898000 $g \times m^{-2} \times d^{-1}$, respectively) with the use of the floating chamber method. The two soil degassing areas of Volcania and Kokkino Nero

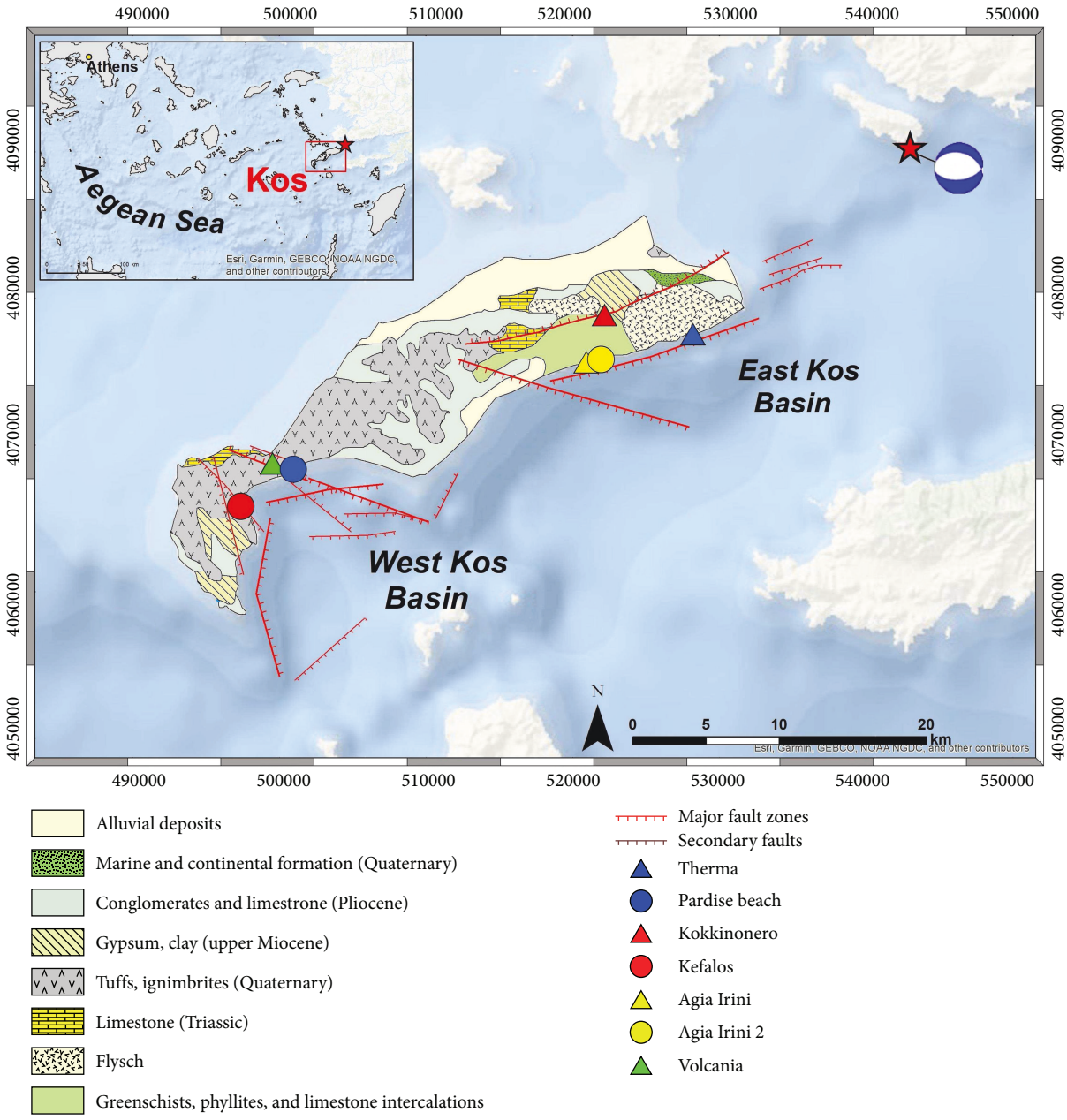

Figure 1: Simplified geological map of the island of Kos (modified after [14, 37]) with the geographical position of the gas sampling points. The earthquake epicenter ($M_w = 6.6$) on the 20th of July 2017 is indicated by a red star. Hypocentral depth (11 km) and focal mechanism are taken from [38].

showed the following median values: 169 g × m^{-2} × d^{-1} and 345 g × m^{-2} × d^{-1}, respectively, whereas the maximum values were 10200 g × m^{-2} × d^{-1} and 14400 g × m^{-2} × d^{-1}, respectively. Due to failure of the temperature probe, the temperature was not measured in the first campaign. Only few measurements were made in the second and third campaigns, and they were mainly concentrated in the highest CO_2 flux measuring points. These measurements were taken at 50 cm in depth and gave values that were approaching the annual mean atmospheric temperature (22°C) excluding significant water vapour upflow at both Volcania and Kokkino Nero.

The portioning method of Sinclair [33] was applied to extract data populations from the dataset. Three main populations, i.e., "background (A)," "intermediate (B)," and "hydrothermal (C)" (Table 2), were identified from the CO_2 flux datasets. The "background" population includes values from 0.1 to~5.8 g × m^{-2} × d^{-1} at Volcania and values from 0.44 to 19 g × m^{-2} × d^{-1} at Kokkino Nero; background population was not identified in the dataset acquired from Therma while at Paradise beach, only the "hydrothermal" population was present. The "intermediate" population includes values from ~6 to 2000 g × m^{-2} × d^{-1} at Volcania, values from 23 to 2500

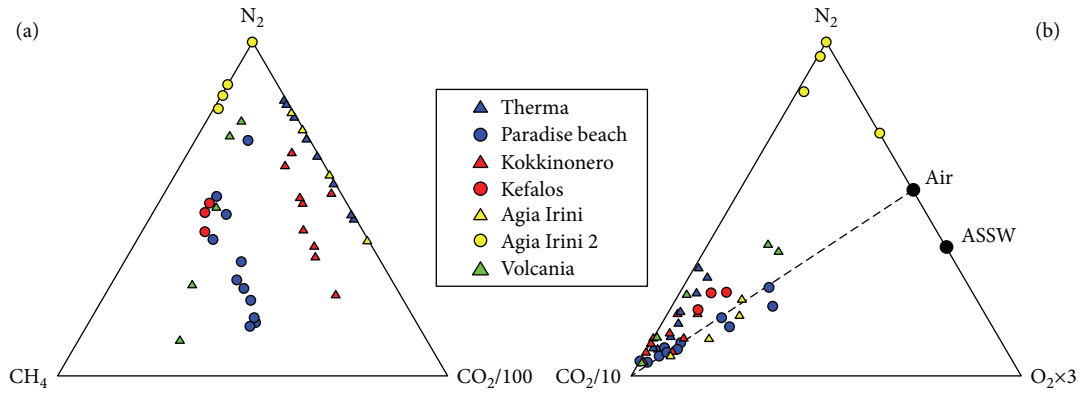

Figure 2: (a) CO_2-N_2-CH_4 and (b) CO_2-N_2-O_2 ternary diagrams. On diagram (b), the typical values of air and ASSW after [39] are also plotted.

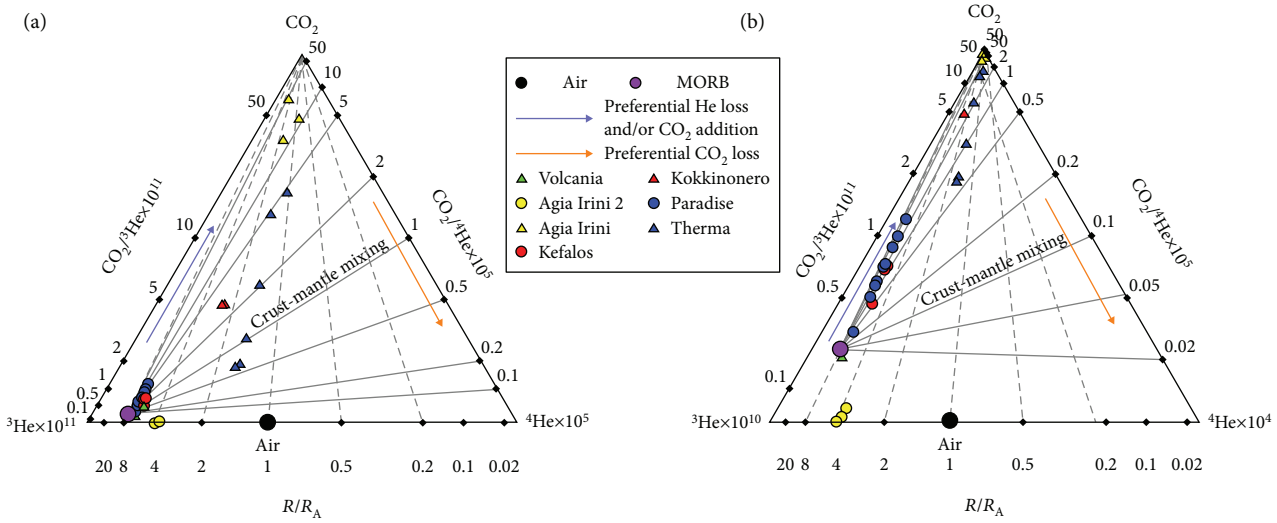

Figure 3: (a) CO_2-^{3}He-^{4}He ternary diagram and (b) CO_2-^{3}He-^{4}He ternary diagram with CO_2 multiplied 10 times. Lines represent mixing lines between mantle-derived and crustal volatiles. Dashed lines show the effects of shallow-level phase separation.

$g \times m^{-2} \times d^{-1}$ at Kokkino Nero, and values from 13 to $150\,g \times m^{-2} \times d^{-1}$ at Therma. The "hydrothermal" population includes values from 2500 to ~$15000\,g \times m^{-2} \times d^{-1}$ at Volcania and Kokkino Nero and values of up to 53100 and $898000\,g \times m^{-2} \times d^{-1}$ for Paradise beach and Therma, respectively.

Table 2 summarizes the number of points contributing to each population of the dataset and the statistical parameters.

According to the identification of background population from the probability plot, the threshold values used for estimation of the CO_2 flux from the Volcania area were $6\,g \times m^{-2} \times d^{-1}$ and $23\,g \times m^{-2} \times d^{-1}$ for Kokkino Nero, while no background value was used for Paradise beach and Therma.

4. Discussion

4.1. Origin of the Gases and Secondary Processes Affecting Their Composition. Carbon dioxide is the carrier phase for mantle-derived fluids. The combination of C and He isotope ratios is a useful tool to evaluate the origin of fluids. Helium isotope ratios are used to distinguish between crustal and upper mantle-derived components. In order to identify general controls on the CO_2 characteristics of Kos island, we plotted the data on a CO_2-^{3}He-^{4}He ternary diagram (Figure 3; [40]). The binary mixing trajectories between MORB-type mantle fluids ($R/R_A = 8$, $CO_2/^3He = 2 \times 10^9$) and various crustal volatile endmembers (0.01 R_A, $CO_2/^3He = 10^{10}$-10^{15}), as well as the general trends expected from addition and/or loss of a particular volatile phase, are also plotted in the diagram. Results propose a mantle origin for He that at points arrives close to the MORB endmember. Samples from Agia Irini and Therma represent products of variable amounts of mixing between mantle-derived and crustal volatiles with a preferential CO_2 addition and/or He loss. On the other hand, Agia Irini 2 is found on the base of the triangle with $CO_2/^3He$ ratios lower than those of the MORB, indicating CO_2 removal, possibly caused by the higher solubility of CO_2 with respect to He in aquatic environments (Figure 3(b)).

For the evaluation of the geologic processes' effects, the CO_2-He data are plotted on the R/R_A vs. $^4He/^{20}Ne$ and

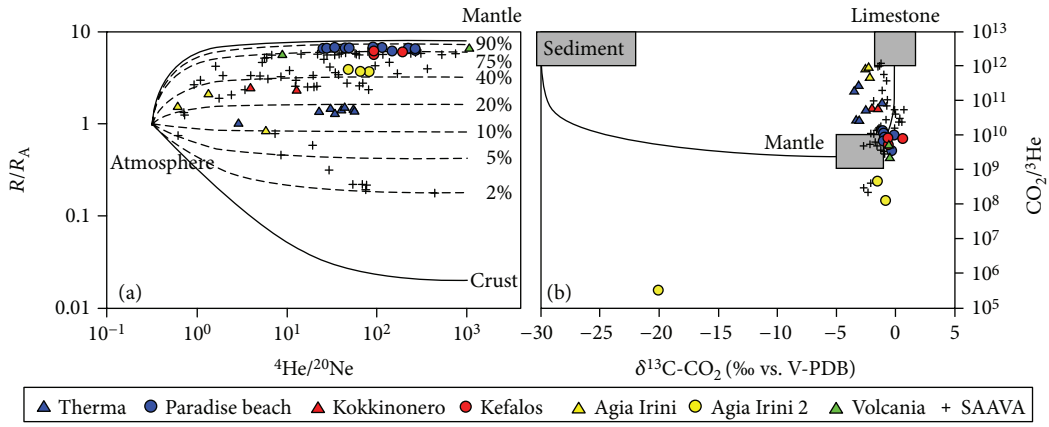

Figure 4: (a) Binary plot of R/R_A vs. $^4He/^{20}Ne$ of the Hellenic gas emissions. The mixing lines between the atmosphere and mantle and between the atmosphere and crust are also plotted. Dashed lines represent mixing between the atmosphere and endmembers, with different percentages of mantle contribution; (b) binary plot of $CO_2/^3He$ vs. $\delta^{13}C\text{-}CO_2$. The compositions for sediments, MORB-like mantle, and limestone endmembers are as follows: $\delta^{13}C\text{-}CO_2 = -30‰$, -5‰, and 0‰, respectively, and $CO_2/^3He = 1 \times 10^{13}$, 2×10^9, and 1×10^{13}, respectively, [41]. SAAVA data from [14, 35, 36, 42–44].

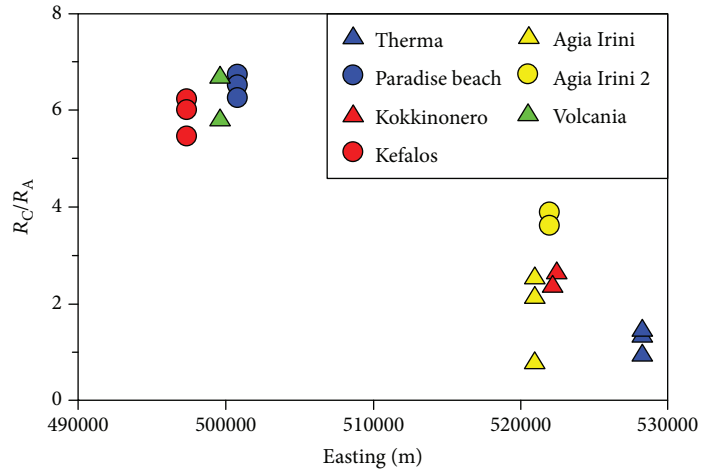

Figure 5: Geographical distribution of the R_C/R_A values of the gas samples collected on Kos island.

$CO_2/^3He$ vs. $\delta^{13}C\text{-}CO_2$ binary diagrams (Figure 4). In the aforementioned diagrams, the binary mixing curves that display the trends drawn by mixtures of the atmospheric component with different mantle and crustal sources [30], as well as the typical values of sediment, limestone, and mantle-derived CO_2 [41], are also plotted. Literature data of gas manifestations along the SAAVA [14, 35, 36, 42–44] are plotted for comparison.

Only few samples show an important atmospheric contribution for He, as they plot close to the atmospheric endmember (Figure 4(a)). Most of the samples display a mixed crustal-mantle contribution always within the range of the SAAVA samples (up to 85% of mantle contribution). In particular, samples from Therma, Kokkino Nero, and Agia Irini present medium to low mantle contributions for He (up to 35% considering a MORB-type source), whereas data of Paradise beach, Kefalos, and Volcania display a relatively higher range (75-80%) with respect to the aforementioned areas.

The distribution of the R_C/R_A values seems to follow a geographical distribution with the highest values collected in the western part of the island, while the lower ones are concentrated in the eastern part (Figure 5). Many volcanic systems show an approximately regular radial distribution of the R/R_A values with the highest values being found close to the main volcanic or geothermal vents. Examples can be found at Nevado del Ruiz [45], Mt. Ontake [46], Lesser Antilles islands [47], Cascades [48], and Mt. Elbrus [49]. Such geographical pattern is generally explained with an increase in the contribution of both crustal (radiogenic) and atmospheric He components when the aquifer water reequilibrates with air, going from the main magmatic feeding system towards the peripheral areas [50]. However, in the present case, no active or recent volcanic conduit can be recognized on the island. Nevertheless, it is worth noting that the westernmost sampled gas manifestations are found along the supposed margin of the caldera that formed after the KPT explosive eruption. Along the margin of this structure, many other volcanic systems have been grown since that eruption (i.e., Nisyros, Strongyli, Pacheia, and Pergousa). It may be therefore hypothesized

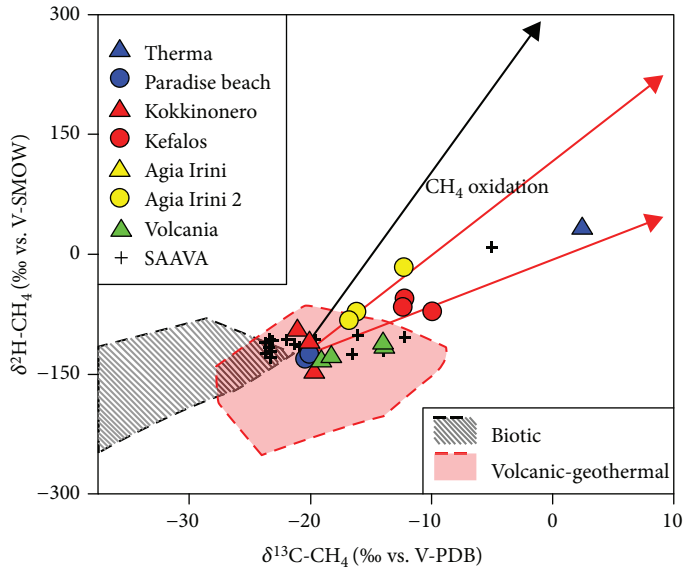

FIGURE 6: Modified Schoell binary diagram [65] of δ^2H-CH_4 and δ^{13}C-CH_4 ratios for the Hellenic gas discharges. Slopes of biogenic oxidation and abiogenic oxidation of CH_4 are plotted as red- and black-colored lines, respectively. SAAVA data from [43].

that the westernmost gas manifestations of Kos are connected to a deep mantle source by the presence of the ring faults of the caldera. At present, in the area, there is no surface sign of thermal anomalies that could point to the presence of a geothermal system possibly fed by an ascending magma batch. On the contrary, the easternmost sampling sites are found away from the caldera margins, mostly along the main tectonic structures, and are, at least in the case of Therma, related to thermal water circulation. Deep-rooted faults frequently constitute channels of high permeability that facilitate the migration of mantle fluids [51]. The strong difference in He isotope composition between the two groups of sampling sites may be explained also with the different geologic substrate of the two areas. In the western part of the island, young volcanic formations prevail, while in the eastern part, mostly older metamorphic rocks crop out. The latter could be the source of the crustal component that lowers the R/R_A values of the gases collected in the eastern part of Kos.

Moreover, gases collected in Kos along with those of SAAVA are found in the mixing line between mantle and limestone endmembers, while the contribution of the organic sediments is trivial (Figure 4(b)). Samples of Paradise beach, Volcania, and Kefalos are those with the highest mantle component showing $CO_2/^3$He ratios similar to those of the MOR gases. Samples collected in Agia Irini 2 present $CO_2/^3$He ratios lower than those of the MOR range indicating a relative CO_2 loss (Figures 3 and 4(b); [52–55]).

Hydrothermal hydrocarbon production can be described by two main mechanisms that deal with the biotic and abiotic origins of methane [56]. Considering this, the origin of CH_4 can be investigated using the classification diagram of Schoell [57, 58]. Thermogenic CH_4 has been reported to exhibit δ^{13}C-CH_4 values that range from -50 to -30‰ and δ^2H-CH_4values ≤ 150‰ (e.g., [57–61]), whereas microbial CH_4 usually has δ^{13}C-CH_4values ≤ 50‰ (e.g., [60–62]).

Samples collected in Kos island as well as samples of the SAAVA [43] plot in the field of volcanic geothermal systems and thus, a geothermal origin is suggested for CH_4 (Figure 6). Exceptions are the samples collected at Kefalos, Agia Irini 2, and Therma, which sometimes present extremely (sample no. 2 of Therma) positive isotope values (for both C and H), pointing to CH_4 oxidation processes. Inorganic oxidation of CH_4 [63] in some samples cannot be ruled out. However, it is noticeable that the isotope fractionations of organic oxidation and inorganic oxidation of CH_4 follow different fractionation paths. The former follows $\Delta H/\Delta C$ slopes ranging from 5.9 to 13 ([64] and references therein) and the latter a slope of 21 [63]. Daskalopoulou et al. [43] considered $\delta^{13}C \approx -21‰$ and $\delta^2H \approx -130‰$ values that cluster the majority of the samples as the most probable values of the isotope composition of geothermal CH_4 in the Greek geothermal systems before oxidation. Based on that, the $\Delta H/\Delta C$ values, comprised between 3.8 and 13.6, are mostly overlapping the typical range of biogenic oxidation processes pointing towards the consumption by methanotrophic microorganisms. It is worth noting that the sites showing signs of methane oxidation are those presenting the lowest gas emission fluxes. The slower uprise of the gases allows a longer interaction with the methanotrophic microorganisms before bubble emission and therefore a higher consumption and a consequent fractionation of methane. This justifies the sometimes-strongly positive values that, considering the abovementioned starting δ^{13}C-CH_4 value, indicate a residual fraction of CH_4 of about 0.4 [61].

4.2. Possible Influence of Seismic Activity on Fluid Geochemistry. Fluids play an important role in earthquake generation by reducing the friction between the fault blocks [66–68] and transporting upper mantle energy with geochemical anomalies that occur before, during, and after earthquakes [69]. Therefore, heat flow and tectonics are

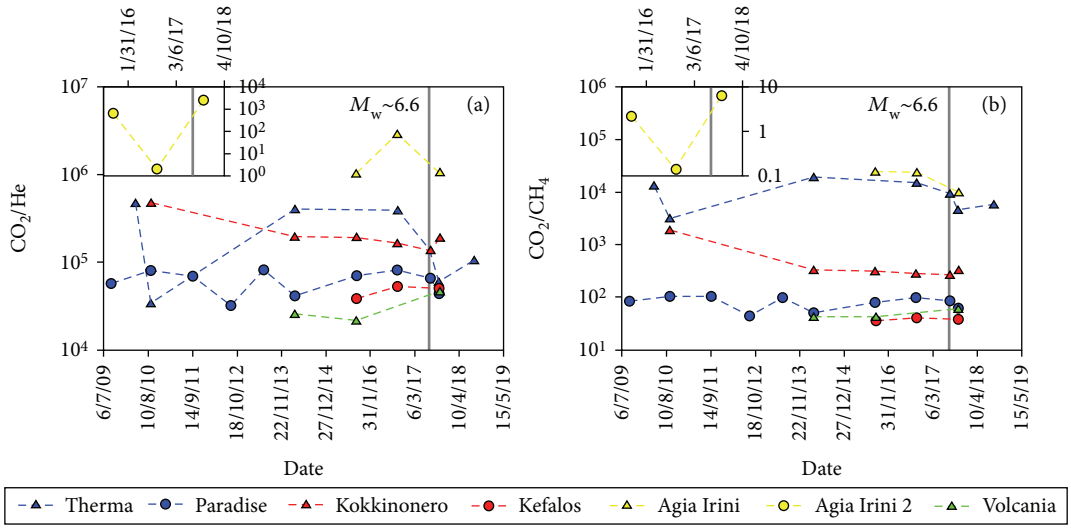

FIGURE 7: Time series plot of (a) $CO_2/^3He$ ratios and (b) CO_2/CH_4 values between 2009 and 2018 in the island of Kos, with the data of Agia Irini 2 being plotted in the inset. The seismic event on the 20th July 2017 is noted with a gray line.

related to both active faults and geothermal anomalies, and for that reason, many earthquake epicenters occur worldwide in areas with elevated heat flow [66, 67]. Many researchers have studied the relations between seismicity and geochemistry and have noticed changes in the physicochemical parameters, the ground deformation, the gas flow rate, and the isotope composition of the gases (e.g., Kobe, Japan [70]; Kamchatka, Russia [71]; El Salvador, Central America [72]; Nisyros, Greece [73]; and Campi Flegrei, Italy [74]).

An earthquake of M_w~6.6 occurred in the Gulf of Gökova between the areas of Bodrum and Kos on the 20th of July 2017. Heavy damages were noticed in both areas with the strongest intensities being recorded in the latter (United States Geological Survey (USGS)). Karasözen et al. [38] attributed this event to a normal fault gently dipping (~37°) northwards. This fault reached the sea bottom along a more than 10 km long E-W trending line generating tsunami waves that added further damages in Kara Ada island, Bodrum, and Kos island [75, 76].

Our campaigns included the systematic gas collection in the period from 2009 to 2018, thus including the seismic event. Three of the sampling sites were specifically resampled on the 26th of July 2017, 6 days after the main shock. In almost each area, results indicate a decrease in CO_2 and an increase in both He and CH_4 concentrations postseismically (Figure 7). This can be explained by a possible CO_2 loss and a consequent relative enrichment of He and CH_4; the difference in solubility may lead to extreme enrichments in the less soluble gases when a gas mixture rises through nonsaturated waters, especially when the gas/water ratio is very low [77]. This is probably the case of the gas collected 10 months before the seismic event at Agia Irini 2.

Furthermore, the collected gases evidenced variations in the R_C/R_A ratios (Figure 8). In particular, all sites but one (Paradise beach), where He isotopes were measured, showed increased R_C/R_A ratios at about 10 months before the earthquake. On the contrary, Paradise beach shows at that time a relative minimum, which is subsequently increased to the highest measured value 6 days after the earthquake. Helium isotopes at Therma present a slightly lower value with respect to the previous and subsequent samples. It is worth mentioning that Therma is the site closest to the epicenter and also the second site presented in this work, where He isotopes were measured 6 days after the seismic event. All seven localities along the island present R_C/R_A ratios greater than those typical for crustal production ($R_C/R_A \approx 0.05$; [78]), revealing the presence of mantle-derived He throughout the fault zones (Table 1; Figures 3 and 4(a)). It is worth noting that all the sampling sites can be related to tectonic structures (Figure 1) that represent a preferential pathway for geogenic degassing. The strain induced by both the impending earthquake and the subsequent aftershock sequence may either induce variations in the permeability of these tectonic structures [79] or induce release of gases from magmatic or geothermal systems [36, 73].

The $\delta^{13}C$-CO_2 values (Figure 8(a)) show also important variations that may be attributed to different processes like

(a) degassing of CO_2 from the geothermal waters that results in both the decrease of the CO_2 contents in the geothermal water and the increase of the $\delta^{13}C$ values of the residual dissolved fraction

(b) addition/dissolution of CO_2 into groundwater, which leads to partial dissolution ($CO_{2(aq)}$), hydration ($HCO_3^-{}_{(aq)}$), and dissociation into HCO_3^- and then CO_3^{2-}. The fractionation factor between $HCO_3^-{}_{(aq)}$ and $CO_{2(g)}$ (ε) is temperature dependent [80–82], and therefore, at temperatures encountered at the sampling localities (<100°C), gaseous CO_2 progresses towards lower $\delta^{13}C$ values with increased dissolution (i.e., decreasing CO_2)

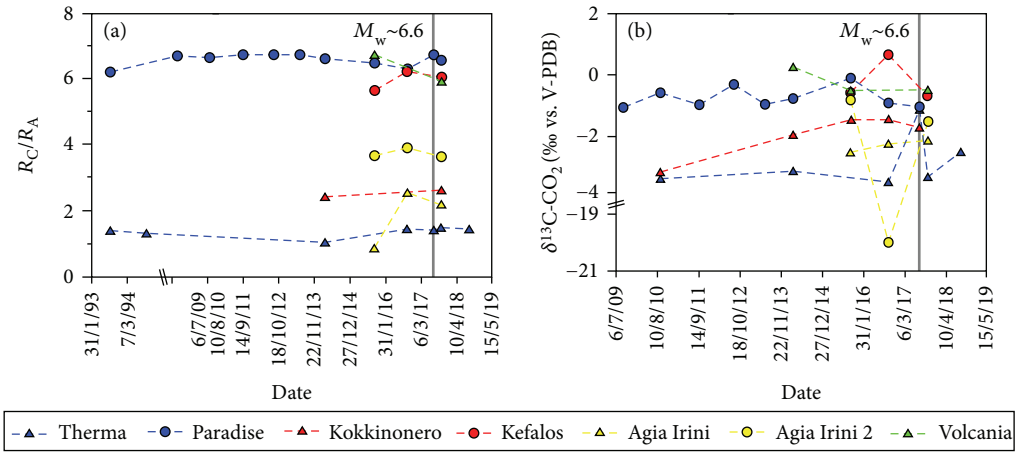

FIGURE 8: Time series plot of (a) R_C/R_A ratios and (b) δ^{13}C-CO$_2$ values between 1993 and 2018 in the island of Kos. In order to eliminate the variable of the atmospheric contamination, the R_C/R_A values were used. The seismic event on the 20th July 2017 is noted with a gray line.

(c) dissolution/precipitation of the mineral calcite, where C isotope values become higher in the solid phase relative to the CO$_2$ in the geothermal water [83] and, consequently, also in this case, δ^{13}C values and CO$_2$ contents decrease in the residual gas phase

(d) mixing of gases with isotopically different CO$_2$

The variation of δ^{13}C-CO$_2$ values in Figure 8(a) is significantly stronger than the variation of R_C/R_A values. A strong decrease in δ^{13}C-CO$_2$ values is observed at Agia Irini 2, 10 months before the seismic event and, coherently with the variations in the chemical composition, may be attributed to CO$_2$ dissolution processes. A reduction in gas upflow rate induced by the impending earthquake can be the cause. Relatively lower δ^{13}C-CO$_2$ values can be noticed also in the samples taken at Paradise beach just before and immediately after the earthquake. Conversely, at other sites, the δ^{13}C values are increasing either slightly and constantly like in the case of Agia Irini and Kokkino Nero or more spike like as seen at Kefalos (10 months before) and Therma (6 days after). None of these variations could be definitely linked to a particular process. Mixing of heavier carbon may derive from fracturing and dissolution of carbonate minerals of the limestones in the sedimentary series or marbles in the metamorphic sequence.

Along with the variations in the chemical and isotope compositions, changes in the degassing areas were also witnessed. In particular, in the submarine manifestations of Paradise beach, the degassing area became wider and a remarkable increase in the flux was observed. Raised water temperatures (at least at Therma) and gas fluxes were also recorded in the areas closer to the epicenter (Therma, Agia Irini, and Agia Irini 2). However, due to the lack of repeated flux measurements and the sometimes-incoherent temporal variations in chemical composition, R_C/R_A and δ^{13}C-CO$_2$, no conclusions regarding the pre- and postseismic changes can be reached in the present work.

4.3. Total CO$_2$ Output Estimation. The CO$_2$ total output estimation is performed following a stocatistic approach obtaining the most probable CO$_2$ output value for each of the three investigated areas (Volcania, Kokkino Nero, and Therma). Such data processing is used to produce the CO$_2$ distribution maps for the three areas (Figure 9).

Analysing the "background" populations extracted from the data, some differences between the datasets are noticed. The background threshold of Volcania is nearly one order of magnitude lower than that obtained from Kokkino Nero. This discrepancy can be referred to the soil assemblage. In fact, the soil at Volcania is more altered and less covered by vegetation even in the low-flux areas with respect to the soil at Kokkino Nero. The strong alteration of the soils in the Volcania area is probably due to past fumarolic activity [19]. The amount of CO$_2$ produced by the biomass at Volcania is lower than that produced at Kokkino Nero, and, consequently, the CO$_2$ threshold value is higher at Kokkino Nero.

The Therma dataset was mainly acquired along the shore with most of the data acquired on the water surface. The biomass producing CO$_2$ in this area was almost absent, and all the CO$_2$ upflow can be addressed to the hydrothermal component. The intermediate population in the Volcania and Kokkino Nero areas represents the mixing of the background component, the hydrothermal component (higher values), and/or the air mixing/dilution (lower values); the intermediate population obtained from the Therma dataset can be addressed to the hydrothermal component mixed with air. As in this site, the CO$_2$ flux is highly sustained reaching the extraordinary value of 898000 $g \times m^{-2} \times d^{-1}$ and the CO$_2$ upflow rate is so high to reduce and in some way prevent the air dilution. Almost all flux measurements included in the hydrothermal population were made with the floating chamber on the water of the artificial pool created for thermal bath purposes. On the contrary, almost all measurements referring to the intermediate population were made on the shores surrounding the pool. The shores are made of highly permeable coarse gravel favouring air circulation. This

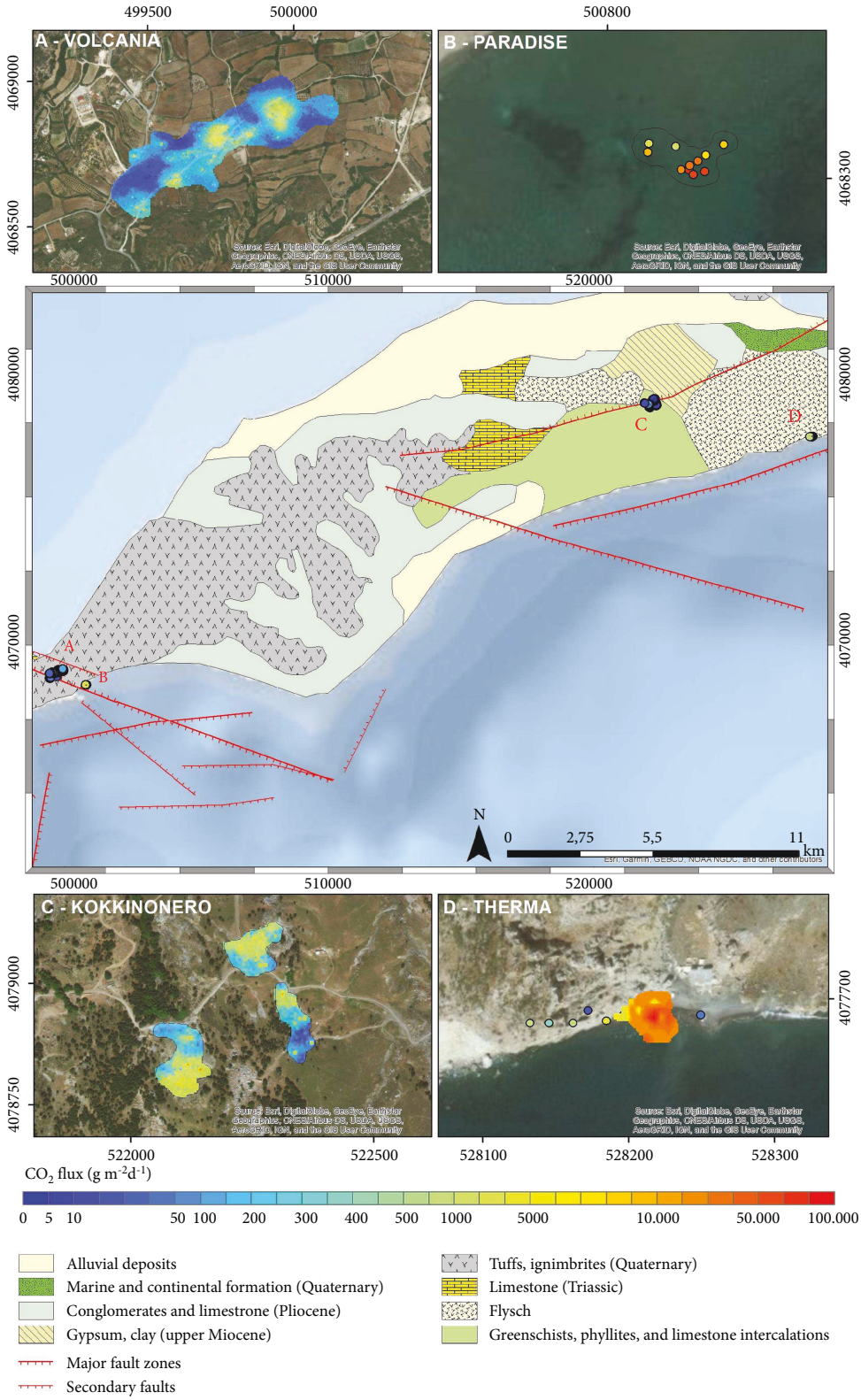

Figure 9: Distribution maps of soil CO_2 flux measurements at Kos. (c) The map of the central part of the island showing all measured points. (a, b, d, and e) Areas with more detailed sample density: Volcania (a), Paradise beach (b), Therma (d), and Kokkino Nero (e).

may explain also the low amount of data included in the intermediate population at Therma and its high upper limit ($3225\,g \times m^{-2} \times d^{-1}$).

The sGs produced an E-type map with the mean expected value for each cell. The total CO_2 output was obtained, for each area, summing all cell values above the threshold

Table 3: CO_2 output estimations.

Site	Area km^2	CO_2 flux[a] $t \times d^{-1}$
Volcania	0.135	24.6
Kokkino Nero	0.250	16.8
Therma	0.0011	20.6
Paradise	0.0006	12.7

[a]The flux is calculated considering only values above the background threshold.

Table 4: CO_2 output from the volcanic/geothermal systems along the SAAVA.

Volcanic system	Reference	$t \times d^{-1}$
Sousaki	[86]	54
Methana	[87]	2.6
Milos	[44]	30.5
Nea Kameni	[31]	15
	[88]	38
Nisyros	[7]	67.8
	[89]	84
Kos	Present work	74.7

multiplied by the surface covered by each cell. The total CO_2 outputs estimated by sGs for Volcania, Kokkino Nero, and Therma are 24.6, 16.8, and 20.6 $t \times d^{-1}$, respectively (Table 3). At Paradise beach, the number of flux measuring points was not enough to produce a map with the sGs method. Therefore, to estimate the CO_2 output of this area, we multiplied the output area by the average of the flux values obtaining a value of 12.7 $t \times d^{-1}$. All the four investigated areas sum up an estimated total CO_2 flux for the island of Kos of about 74.7 $t \times d^{-1}$. Such value falls within the range reported for the other volcanic/geothermal systems along the SAAVA (Table 4) where outputs as low as 2.6 (Methana) and up to 84 $t \times d^{-1}$ (Nisyros) have been obtained. All these values fall at the lower end of the output estimations of volcanic systems worldwide [84, 85] and typical of quiescent volcanic systems.

5. Conclusions

Gas emissions are spread over the volcanic island of Kos and are expressed as hot springs, underwater bubbling, and sulfate salt efflorescence. Results have proposed a mixed mantle-limestone origin for CO_2, which is the prevailing gas species, whereas an up to 85% mantle contribution has been recognized for He. Gas components such as H_2, H_2S, and CH_4 have indicated a geothermal origin within a still not recognized reservoir beneath the island. Gas manifestations as well as anomalous degassing areas can be related to important tectonic structures. The active tectonics of the area often results in seismic activity with the recent earthquake (20th July 2017—M_w~6.6) causing a tsunami phenomenon and heavy damages on the island. Variations in both the chemical and isotope compositions and changes in the degassing areas and the physicochemical parameters of the systems have been observed. These have been possibly caused due to changes in mixing ratios of fluids of different origins and in the flux of uprising gases, although it has not been made possible to interpret all variations univocally.

The four main degassing areas (Volcania, Paradise beach, Kokkino Nero, and Therma) that have been recognized present sometimes very high flux values ($>10^5$ $g \times m^{-2} \times d^{-1}$). The total CO_2 output for Kos has been estimated in 74.7 $t \times d^{-1}$. This estimation has been in the range of values typical for the volcanic geothermal systems along the SAAVA and in the lower end of the worldwide volcanic output estimations

Data Availability

The data on gas geochemistry used to support the findings of this study are included within the article. The CO_2 flux data are included within the supplementary information file.

Conflicts of Interest

The authors declare that they have no conflicts of interest.

Acknowledgments

We kindly acknowledge the help of the Marine warrant officer Ilias Simadakis who gave us the permission to collect samples, the owner of "Kardamena Watersports Center" Mr. Nikos Nikolakopoulos who gave us one of his boats, and Mr. Yannis Limperis who accompanied us to the points of interest. CO_2 flux measurements would have not been possible without the friendly help of Salvatore Inguaggiato who gave us the device that he manages. All analyses were made at the laboratories of the INGV of Palermo, and we are grateful to all the following laboratories responsibles and technicians: G. Capasso, F. Grassa, M. Martelli, Y. Oliveri, A. Rizzo, F. Salerno, A. Sollami, and M. Tantillo.

Supplementary Materials

MS Office Excel file "Table S1" containing the coordinates and the values of all the CO_2 flux measurements made on the island of Kos. *(Supplementary Materials)*

References

[1] J. Jackson, "Rates of active deformation in the Eastern Mediterranean," in *Recent Evolution and Seismicity of the Mediterranean Region. NATO ASI Series (Series C: Mathematical and Physical Sciences), vol 402*, pp. 53–64, Springer, Dordrecht, 1993.

[2] M. J. R. Wortel and W. Spakman, "Subduction and slab detachment in the Mediterranean-Carpathian region," *Science*, vol. 290, no. 5498, pp. 1910–1917, 2000.

[3] D. McKenzie, "Active tectonics of the Mediterranean region," *Geophysical Journal International*, vol. 30, no. 2, pp. 109–185, 1972.

[4] M. Fytikas, F. Innocenti, P. Manetti, A. Peccerillo, R. Mazzuoli, and L. Villari, "Tertiary to Quaternary evolution of volcanism in the Aegean region," *Geological Society London Special Publications*, vol. 17, no. 1, pp. 687–699, 1985.

[5] G. Pe-Piper and D. J. W. Piper, *The Igneous Rocks of Greece*, Gebrüder Borntreager, Berlin, 2002.

[6] G. A. Papadopoulos, M. Sachpazi, G. Panopoulou, and G. Stavrakakis, "The volcanoseismic crisis of 1996-1997 in Nisyros, SE Aegean Sea, Greece," *Terra Nova*, vol. 10, no. 3, pp. 151–154, 1998.

[7] S. Caliro, G. Chiodini, D. Galluzzo et al., "Recent activity of Nisyros volcano (Greece) inferred from structural, geochemical and seismological data," *Bulletin of Volcanology*, vol. 67, no. 4, pp. 358–369, 2005.

[8] J. Gottsmann, H. Rymer, and L. K. Wooller, "On the interpretation of gravity variations in the presence of active hydrothermal systems: insights from the Nisyros caldera, Greece," *Geophysical Research Letters*, vol. 32, no. 23, 2005.

[9] E. Lagios, V. Sakkas, I. Parcharidis, and V. Dietrich, "Ground deformation of Nisyros volcano (Greece) for the period 1995–2002: results from DInSAR and DGPS observations," *Bulletin of Volcanology*, vol. 68, no. 2, pp. 201–214, 2005.

[10] G. Pe-Piper, D. J. W. Piper, and C. Perissoratis, "Neotectonics and the Kos Plateau Tuff eruption of 161 ka, South Aegean arc," *Journal of Volcanology and Geothermal Research*, vol. 139, no. 3–4, pp. 315–338, 2005.

[11] X. Le Pichon and J. Angelier, "The Hellenic arc and trench system: a key to the neotectonic evolution of the Eastern Mediterranean area," *Tectonophysics*, vol. 60, no. 1-2, pp. 1–42, 1979.

[12] D. J. Papanikolaou, "Geotectonic evolution of the Aegean," *Bulletin of Geological Society of Greece*, vol. 18, pp. 33–48, 1993.

[13] J. Jackson, "Active tectonics of the Aegean region," *Annual Review of Earth and Planetary Sciences*, vol. 22, no. 1, pp. 239–271, 1994.

[14] G. La Ruffa, C. Panichi, T. Kavouridis, V. Liberopoulou, J. Leontiadis, and A. Caprai, "Isotope and chemical assessment of geothermal potential of Kos island, Greece," *Geothermics*, vol. 28, no. 2, pp. 205–217, 1999.

[15] D. J. W. Piper, G. Pe-Piper, and D. Lefort, "Precursory activity of the 161 ka Kos Plateau Tuff eruption, Aegean Sea (Greece)," *Bulletin of Volcanology*, vol. 72, no. 6, pp. 657–669, 2010.

[16] E. Lagios, D. Galanopoulos, B. A. Hobbs, and G. J. K. Dawes, "Two-dimensional magnetotelluric modelling of the Kos island geothermal region (Greece)," *Tectonophysics*, vol. 287, no. 1-4, pp. 157–172, 1998.

[17] D. J. Papanikolaou and E. Lekkas, *Miocene Tectonism in Kos, Dodecanese Islands*, IESCA Abstract, Izmir, 1990.

[18] O. Bachmann, "The petrologic evolution and pre-eruptive conditions of the rhyolitic Kos Plateau Tuff (Aegean arc)," *Central European Journal of Geosciences*, vol. 2, no. 3, pp. 270–305, 2010.

[19] J.-M. Bardintzeff, P. Dalabakis, H. Traineau, and R. Brousse, "Recent explosive volcanic episodes on the island of Kos (Greece): associated hydrothermal parageneses and geothermal area of Volcania," *Terra Research*, vol. 1, no. 1, pp. 75–78, 1988.

[20] S. Varnavas, D. Panagiotaras, and P. Megalovasilis, "Chemical characteristics of a submarine hydrothermal system offshore Kos island, on the Hellenic volcanic arc," *Rapports et Procès Verbaux de la Commission Internationale Pour L'Exploration Scientifique de la mer Mediterranee*, vol. 35, no. 1, pp. 104-105, 1998.

[21] V. Hatzivasileiou, *History of Island of Kos Ancient, Medieval and Modern*, Municipality of Kos, Kos Greece, 2013.

[22] P. Delmelle and J. Stix, "Volcanic gases," in *Encyclopedia of Volcanoes*, pp. 877–896, Academic Press, 1999.

[23] W. C. Evans, M. L. Sorey, B. M. Kennedy, D. A. Stonestrom, J. D. Rogie, and D. L. Shuster, "High CO_2 emissions through porous media: transport mechanisms and implications for flux measurement and fractionation," *Chemical Geology*, vol. 177, no. 1-2, pp. 15–29, 2001.

[24] A. Mazzini, H. Svensen, S. Planke et al., "When mud volcanoes sleep: insight from seep geochemistry at the Dashgil mud volcano, Azerbaijan," *Marine and Petroleum Geology*, vol. 26, no. 9, pp. 1704–1715, 2009.

[25] W.-L. Hong, G. Etiope, T. F. Yang, and P.-Y. Chang, "Methane flux from miniseepage in mud volcanoes of SW Taiwan: comparison with the data from Italy, Romania, and Azerbaijan," *Journal of Asian Earth Sciences*, vol. 65, pp. 3–12, 2013.

[26] J. L. Lewicki and S. L. Brantley, "CO_2 degassing along the San Andreas Fault, Parkfield, California," *Geophysical Research Letters*, vol. 27, no. 1, pp. 5–8, 2000.

[27] G. Yüce, C. C. Fu, W. D'Alessandro et al., "Geochemical characteristics of soil radon and carbon dioxide within the Dead Sea Fault and Karasu Fault in the Amik Basin (Hatay), Turkey," *Chemical Geology*, vol. 469, pp. 129–146, 2017.

[28] D. Granieri, R. Avino, and G. Chiodini, "Carbon dioxide diffuse emission from the soil: ten years of observations at Vesuvio and Campi Flegrei (Pozzuoli), and linkages with volcanic activity," *Bulletin of Volcanology*, vol. 72, no. 1, pp. 103–118, 2010.

[29] F. Viveiros, C. Cardellini, T. Ferreira, S. Caliro, G. Chiodini, and C. Silva, "Soil CO_2 emissions at Furnas volcano, São Miguel Island, Azores archipelago: volcano monitoring perspectives, geomorphologic studies, and land use planning application," *Journal of Geophysical Research*, vol. 115, no. B12, 2010.

[30] Y. Sano and H. Wakita, "Geographical distribution of $^3He/^4He$ ratios in Japan: implications for arc tectonics and incipient magmatism," *Journal of Geophysical Research*, vol. 90, no. B10, pp. 8729–8741, 1985.

[31] G. Chiodini, R. Cioni, M. Guidi, B. Raco, and L. Marini, "Soil CO_2 flux measurements in volcanic and geothermal areas," *Applied Geochemistry*, vol. 13, no. 5, pp. 543–552, 1998.

[32] J. L. Lewicki, D. Bergfeld, C. Cardellini et al., "Comparative soil CO_2 flux measurements and geostatistical estimation methods on Masaya volcano, Nicaragua," *Bulletin of Volcanology*, vol. 68, no. 1, pp. 76–90, 2005.

[33] A. J. Sinclair, "Selection of threshold values in geochemical data using probability graphs," *Journal of Geochemical Exploration*, vol. 3, no. 2, pp. 129–149, 1974.

[34] C. V. Deutsch and A. G. Journel, *GSLIB: Geostatistical Software Library and User's Guide*, Oxford University Press, New York, NY, USA, 2nd edition, 1998.

[35] A. Minissale, V. Duchi, N. Kolios, M. Nocenti, and C. Verrucchi, "Chemical patterns of thermal aquifers in the volcanic islands of the Aegean arc, Greece," *Geothermics*, vol. 26, no. 4, pp. 501–518, 1997.

[36] A. Shimizu, H. Sumino, K. Nagao, K. Notsu, and P. Mitropoulos, "Variation in noble gas isotopic composition

of gas samples from the Aegean arc, Greece," *Journal of Volcanology and Geothermal Research*, vol. 140, no. 4, pp. 321–339, 2005.

[37] P. Nomikou and D. Papanikolaou, "Extension of active fault zones on Nisyros volcano across the Yali-Nisyros Channel based on onshore and offshore data," *Marine Geophysical Research*, vol. 32, no. 1-2, pp. 181–192, 2011.

[38] E. Karasözen, E. Nissen, P. Büyükakpınar et al., "The 2017 July 20 Mw 6.6 Bodrum–Kos earthquake illuminates active faulting in the Gulf of Gökova, SW Turkey," *Geophysical Journal International*, vol. 214, no. 1, pp. 185–199, 2018.

[39] R. Kipfer, W. Aeschbach-Hertig, F. Peeters, and M. Stute, "Noble gases in lakes and ground waters," *Reviews in Mineralogy and Geochemistry*, vol. 47, no. 1, pp. 615–700, 2002.

[40] W. F. Giggenbach, Y. Sano, and H. Wakita, "Isotopic composition of helium and CO_2 and CH_4 contents in gases produced along the New Zealand part of a convergent plate boundary," *Geochimica et Cosmochimica Acta*, vol. 57, no. 14, pp. 3427–3455, 1993.

[41] Y. Sano and B. Marty, "Origin of carbon in fumarolic gas from island arcs," *Chemical Geology*, vol. 119, no. 1-4, pp. 265–274, 1995.

[42] A. L. Rizzo, A. Caracausi, V. Chavagnac et al., "Kolumbo submarine volcano (Greece): an active window into the Aegean subduction system," *Scientific Reports*, vol. 6, no. 1, article 28013, 2016.

[43] K. Daskalopoulou, S. Calabrese, F. Grassa et al., "Origin of methane and light hydrocarbons in natural fluid emissions: a key study from Greece," *Chemical Geology*, vol. 479, pp. 286–301, 2018.

[44] K. Daskalopoulou, A. L. Gagliano, S. Calabrese et al., "Gas geochemistry and CO_2 output estimation at the island of Milos, Greece," *Journal of Volcanology and Geothermal Research*, vol. 365, pp. 13–22, 2018.

[45] Y. Sano, H. Wakita, and S. N. Williams, "Helium isotope systematics at Nevado del Ruiz volcano, Colombia: implications for the volcanic hydrothermal system," *Journal of Volcanology and Geothermal Research*, vol. 42, no. 1-2, pp. 41–52, 1990.

[46] Y. Sano, Y. Nishio, S. Sasaki, T. Gamo, and K. Nagao, "Helium and carbon isotope systematics at Ontake volcano, Japan," *Journal of Geophysical Research*, vol. 103, no. B10, pp. 23863–23873, 1998.

[47] P. Jean-Baptiste, P. Allard, E. Fourré, F. Parello, and A. Aiuppa, "Helium isotope systematics of volcanic gases and thermal waters of Guadeloupe island, Lesser Antilles," *Journal of Volcanology and Geothermal Research*, vol. 283, pp. 66–72, 2014.

[48] M. O. Saar, M. C. Castro, C. M. Hall, M. Manga, and T. P. Rose, "Quantifying magmatic, crustal, and atmospheric helium contributions to volcanic aquifers using all stable noble gases: implications for magmatism and groundwater flow," *Geochemistry, Geophysics, Geosystems*, vol. 6, no. 3, 2005.

[49] B. G. Polyak, V. Y. Lavrushin, and I. L. Kamensky, "Mantle helium traces in the Elbrus–Kazbek sector of the Greater Caucasus and adjacent areas," *Chemical Geology*, vol. 266, no. 1-2, pp. 57–66, 2009.

[50] Y. Sano and T. P. Fischer, "The analysis and interpretation of noble gases in modern hydrothermal systems," in *The Noble Gases as Geochemical Tracers*, pp. 249–317, Springer-Verlag, Berlin Heidelberg, 2013.

[51] A. Paonita, M. Longo, S. Bellomo, W. D'Alessandro, and L. Brusca, "Dissolved inert gases (He, Ne and N_2) as markers of groundwater flow and degassing areas at Mt Etna volcano (Italy)," *Chemical Geology*, vol. 443, pp. 10–21, 2016.

[52] C. J. Ballentine, R. Burgess, and B. Marty, "Tracing fluid origin, transport and interaction in the crust," *Reviews in Mineralogy and Geochemistry*, vol. 47, no. 1, pp. 539–614, 2002.

[53] C. J. Ballentine, M. Schoell, D. Coleman, and B. A. Cain, "300-Myr-old magmatic CO_2 in natural gas reservoirs of the West Texas Permian basin," *Nature*, vol. 409, no. 6818, pp. 327–331, 2001.

[54] B. Sherwood Lollar, C. J. Ballentine, and R. K. Onions, "The fate of mantle-derived carbon in a continental sedimentary basin: integration of CHe relationships and stable isotope signatures," *Geochimica et Cosmochimica Acta*, vol. 61, no. 11, pp. 2295–2307, 1997.

[55] B. Sherwood Lollar, R. K. O'Nions, and C. J. Ballentine, "Helium and neon isotope systematics in carbon dioxide-rich and hydrocarbon-rich gas reservoirs," *Geochimica et Cosmochimica Acta*, vol. 58, no. 23, pp. 5279–5290, 1994.

[56] Y. Taran and W. Giggenbach, "Geochemistry of light hydrocarbons in subduction-related volcanic and hydrothermal fluids," *Society of Economic Geologists Special Publication*, vol. 10, no. 6, pp. 61–74, 2003.

[57] M. Schoell, "The hydrogen and carbon isotopic composition of methane from natural gases of various origins," *Geochimica et Cosmochimica Acta*, vol. 44, no. 5, pp. 649–661, 1980.

[58] M. Schoell, "Multiple origins of methane in the Earth," *Chemical Geology*, vol. 71, no. 1-3, pp. 1–10, 1988.

[59] A. S. Bradley and R. E. Summons, "Multiple origins of methane at the Lost City hydrothermal field," *Earth and Planetary Science Letters*, vol. 297, no. 1-2, pp. 34–41, 2010.

[60] M. J. Whiticar, "Stable isotope geochemistry of coals, humic kerogens and related natural gases," *International Journal of Coal Geology*, vol. 32, no. 1-4, pp. 191–215, 1996.

[61] M. J. Whiticar, "Carbon and hydrogen isotope systematics of bacterial formation and oxidation of methane," *Chemical Geology*, vol. 161, no. 1-3, pp. 291–314, 1999.

[62] T. M. McCollom and J. S. Seewald, "Abiotic synthesis of organic compounds in deep-sea hydrothermal environments," *Chemical Reviews*, vol. 107, no. 2, pp. 382–401, 2007.

[63] Y. Kiyosu and S. Imaizumi, "Carbon and hydrogen isotope fractionation during oxidation of methane by metal oxides at temperatures from 400° to 530°C," *Chemical Geology*, vol. 133, no. 1-4, pp. 279–287, 1996.

[64] S. B. Cadieux, J. R. White, P. E. Sauer, Y. Peng, A. E. Goldman, and L. M. Pratt, "Large fractionations of C and H isotopes related to methane oxidation in Arctic lakes," *Geochimica et Cosmochimica Acta*, vol. 187, pp. 141–155, 2016.

[65] G. Etiope and M. Schoell, "Abiotic gas: atypical but not rare," *Elements*, vol. 10, no. 4, pp. 291–296, 2014.

[66] J. Du, W. Cheng, Y. Zhang et al., "Helium and carbon isotopic compositions of thermal springs in the earthquake zone of Sichuan, Southwestern China," *Journal of Asian Earth Sciences*, vol. 26, no. 5, pp. 533–539, 2006.

[67] J. Du, Y. Xu, and M. Sun, "$^3He/^4He$ and heat flow in oil gas bearing basins, China's mainland," *Chinese Journal of Geophysics*, vol. 14, no. 2, pp. 239–247, 1998.

[68] S. A. Miller, Y. Ben-Zion, and J. P. Burg, "A three-dimensional fluid-controlled earthquake model: behavior and

implications," *Journal of Geophysical Research*, vol. 104, no. B5, pp. 10621–10638, 1999.

[69] T. Rikitake, *Earthquake Forecasting and Warning*, Center for Academic Publications, Tokyo, 1982.

[70] C. Y. King, N. Koizumi, and Y. Kitagawa, "Hydrogeochemical anomalies and the 1995 Kobe earthquake," *Science*, vol. 269, no. 5220, pp. 38-39, 1995.

[71] S. P. Kingsley, P. F. Biagi, R. Piccolo et al., "Hydrogeochemical precursors of strong earthquakes: a realistic possibility in Kamchatka," *Physics and Chemistry of the Earth, Part C: Solar, Terrestrial & Planetary Science*, vol. 26, no. 10-12, pp. 769–774, 2001.

[72] G. Chiodini, "CO_2/CH_4 ratio in fumaroles a powerful tool to detect magma degassing episodes at quiescent volcanoes," *Geophysical Research Letters*, vol. 36, no. 2, 2009.

[73] J. M. L. Salazar, N. M. Pérez, P. A. Hernández et al., "Precursory diffuse carbon dioxide degassing signature related to a 5.1 magnitude earthquake in El Salvador, Central America," *Earth and Planetary Science Letters*, vol. 205, no. 1–2, pp. 81–89, 2002.

[74] G. Chiodini, J. Selva, E. Del Pezzo et al., "Clues on the origin of post-2000 earthquakes at Campi Flegrei caldera (Italy)," *Scientific Reports*, vol. 7, no. 1, p. 4472, 2017.

[75] M. Heidarzadeh, O. Necmioglu, T. Ishibe, and A. C. Yalciner, "Bodrum–Kos (Turkey-Greece) Mw 6.6 earthquake and tsunami of 20 July 2017: a test for the Mediterranean tsunami warning system," *Geoscience Letters*, vol. 4, no. 1, 2017.

[76] A. Yalçıner, A. Annunziato, G. Papadopoulos et al., *The 20th July 2017 (22:31 UTC) Bodrum-Kos Earthquake and Tsunami: Post Tsunami Field Survey Report*, Technical Report Middle East Technical University, 2017.

[77] W. D'Alessandro, L. Brusca, K. Kyriakopoulos, S. Bellomo, and S. Calabrese, "A geochemical traverse along the "Sperchios Basin — Evoikos Gulf" Graben (Central Greece): origin and evolution of the emitted fluids," *Marine and Petroleum Geology*, vol. 55, pp. 295–308, 2014.

[78] J. N. Andrews, "The isotopic composition of radiogenic helium and Its use to study groundwater movement in confined aquifers," *Chemical Geology*, vol. 49, no. 1-3, pp. 339–351, 1985.

[79] G. Chiodini, C. Cardellini, A. Amato et al., "Carbon dioxide Earth degassing and seismogenesis in central and southern Italy," *Geophysical Research Letters*, vol. 31, no. 7, 2004.

[80] I. Wendt, "Fractionation of carbon isotopes and its temperature dependence in the system CO_2-gas-CO_2 in solution and HCO_3–CO_2 in solution," *Earth and Planetary Science Letters*, vol. 4, no. 1, pp. 64–68, 1968.

[81] J. Zhang, P. D. Quay, and D. O. Wilbur, "Carbon isotope fractionation during gas–water exchange and dissolution of CO_2," *Geochimica et Cosmochimica Acta*, vol. 59, no. 1, pp. 107–114, 1995.

[82] J. Szaran, "Achievement of carbon isotope equilibrium in the system HCO_3^- (solution) - CO_2 (gas)," *Chemical Geology*, vol. 142, no. 1-2, pp. 79–86, 1997.

[83] K. Emrich, D. H. Ehhalt, and J. C. Vogel, "Carbon isotope fractionation during the precipitation of calcium carbonate," *Earth and Planetary Science Letters*, vol. 8, no. 5, pp. 363–371, 1970.

[84] G. Pecoraino, L. Brusca, W. D'Alessandro, S. Giammanco, S. Inguaggiato, and M. Longo, "Total CO_2 output from Ischia island volcano (Italy)," *Geochemical Journal*, vol. 39, no. 5, pp. 451–458, 2005.

[85] S. Inguaggiato, A. Mazot, I. S. Diliberto et al., "Total CO_2 output from Vulcano island (Aeolian Islands, Italy)," *Geochemistry, Geophysics, Geosystems*, vol. 13, no. 2, 2012.

[86] W. D'Alessandro, L. Brusca, K. Kyriakopoulos et al., "Diffuse and focused carbon dioxide and methane emissions from the Sousaki geothermal system, Greece," *Geophysical Research Letters*, vol. 33, no. 5, 2006.

[87] W. D'Alessandro, L. Brusca, K. Kyriakopoulos, G. Michas, and G. Papadakis, "Methana, the westernmost active volcanic system of the South Aegean arc (Greece): insight from fluids geochemistry," *Journal of Volcanology and Geothermal Research*, vol. 178, no. 4, pp. 818–828, 2008.

[88] M. M. Parks, S. Caliro, G. Chiodini et al., "Distinguishing contributions to diffuse CO_2 emissions in volcanic areas from magmatic degassing and thermal decarbonation using soil gas ^{222}Rn–$\delta^{13}C$ systematics: application to Santorini volcano, Greece," *Earth and Planetary Science Letters*, vol. 377-378, pp. 180–190, 2013.

[89] C. Cardellini, G. Chiodini, and F. Frondini, "Application of stochastic simulation to CO_2 flux from soil: mapping and quantification of gas release," *Journal of Geophysical Research Atmospheres*, vol. 108, no. B9, article 2425, 2003.